Left Ventricular Pressure-Volume Analysis : an example of function assessment on a sheep

Dima Rodriguez

▶ **To cite this version:**

Dima Rodriguez. Left Ventricular Pressure-Volume Analysis : an example of function assessment on a sheep. [Research Report] Université Paris Sud. 2015. hal-01123722

HAL Id: hal-01123722
https://hal.science/hal-01123722

Submitted on 5 Mar 2015

HAL is a multi-disciplinary open access archive for the deposit and dissemination of scientific research documents, whether they are published or not. The documents may come from teaching and research institutions in France or abroad, or from public or private research centers.

L'archive ouverte pluridisciplinaire **HAL**, est destinée au dépôt et à la diffusion de documents scientifiques de niveau recherche, publiés ou non, émanant des établissements d'enseignement et de recherche français ou étrangers, des laboratoires publics ou privés.

Research Report

Dima Rodriguez

Left Ventricular Pressure-Volume Analysis

an example of function assessment on a sheep

2010

Imagerie par Résonance Magnétique Médicale et Mulitmodalité

Left Ventricular Pressure-Volume Analysis: an example of function assessment on a sheep

Dima Rodriguez
dima.rodriguez@u-psud.fr

2010

A short version of this work is published in Medical Engineering and Physics Vol. 37, Issue 1, January 2015, pp.100–108

1 Introduction

The evaluation of the left ventricle (LV) performance is of high importance in physiologic investigation and clinical practice. The diastolic LV function can be assessed by measurements of the ventricular pressure decline and filling, reflecting relaxation properties, as well as the relationship between pressure and volume during diastole which characterizes stiffness. As for the systolic LV performance, it is governed by three principal factors, preload, afterload and the contractile or inotropic state of the myocardium. Preload defines the load on the myocardial fibers just prior to contraction, i.e. the amount of blood in the ventricle at the end of diastole, while afterload is determined by the external factors that oppose the shortening of muscle fibers, i.e. arterial impedance. Preload and afterload determinants can be relatively easily measured or evaluated, but assessing contractile state is far more difficult. Any index intended to reflect contractility must be load independent.

Common studies evaluate contractility using left ventricular stroke volume (SV), ejection fraction (EF) and cardiac output (CO). Though intuitive and simple, these parameters are load-dependent and consequently represent poor contractility indexes. For instance, they are not good indicators of heart failure and cardiac dysfunction [1, 2].Other studies rely on pressure measurements alone to assess the LV performance. They evaluate, for example, the maximum rate of pressure change (dP/dt_{max}) which is known to be sensitive to inotropic state and thus correlates with cardiac contractility. Nonetheless, its load-dependence [3, 4, 5] makes it a weak contractility indicator. The peak decline of pressure (dP/dt_{min}), on the other hand, can quantify isovolumic relaxation, but it cannot be qualified as an intrinsic relaxation index since it is preload-dependent [6] as well as afterload-dependent [7]. A widely used parameter for the relaxation quantification is the time constant τ which characterizes the pressure decay during isovolumic relaxation. Despite being preload-independent [8], τ cannot be considered an ideal index because of its afterload dependence.

No perfect assessment index can be obtained from volume or pressure alone. Indeed, volume or pressure measurements on their own are not sufficient to characterize the systolic performance, they cannot solely define contractility and cardiac response to inotropic agents. Simultaneous pressure and volume measurements are necessary to provide valuable functional parameters. Pressure indexes can thus be coupled with volume information to negate load dependence. For example, rather than considering dP/dt_{max}, the relationship of this value to end diastolic volume (EDV) can be

computed by varying preload conditions. This relationship is linear and its slope provides a preload-independent contractility index [9]. The relaxation constant τ can also be evaluated over a range of afterloads and plotted against EDV [10].

In addition, a wide variety of indexes that can be quantified by analyzing pressure-volume (PV) loops have been proposed to characterize the left ventricle systolic and diastolic performance. For instance a straightforward characterization of the myocardium stiffness can be obtained from the slope of the pressure-volume relationship during diastole. Furthermore, a measurement of the ventricular elastance when the contractile forces in the ventricle are at their peak, constitutes a good indicator of the ventricular contractility and systolic function. Known as end-systolic elastance E_{es}, it is independent of preload, afterload and heart rate [11, 12]. The arterial system, as afterload, can also be assessed from the PV loop, and, like the ventricle chamber, it can be characterized by its elastance E_a. Studies have shown the importance of E_a as a descriptor of the vascular load and its impact on cardiac performance [13, 14], indicating that the ratio E_a/E_{es} quantifies the coupling between the ventricle and arterial system and governs ventriculoarterial matching. Additionally, PV loop area analysis can provide an evaluation of mechanical energies of a ventricular beat and an assessment of the LV efficiency.

To measure the ventricle volume, the conductance catheter technique has been used extensively, it is based on the electrical conductance of the blood contained in the cavity. This technique, nonetheless, is based on geometric assumptions, needs volume-dependent calibration and is limited by the non-linearity of the conductance-volume relation when large volume changes are involved [15]. Furthermore, it relies on Ohm's law which might not be fully appropriate due to the non-uniformity of the composition of ventricle and blood, and uses correction parameters that are error prone due to ventricle geometry and wall thickness changes during contraction [16]. Volume assessment using cine MRI were proven to yield a more accurate and reliable estimate [16, 17]. For PV loop construction simultaneous volume and pressure measurements are necessary, but given the magnetic nature of standard pressure sensors, this is problematic during MRI. The pressure signal would be contaminated by the MR environment and the presence of the sensor would produce artifacts on the image.

In this report we present a feasibility study for simultaneous pressure measurements using optical sensors during MRI. In vivo measurements on a sheep are performed and pressure-volume loops are derived by combining MRI-estimated ventricular volumes with on-site pressure measurements for various inotropic states. The usual functional indexes are computed, and PV loop analysis is performed to evaluate the response to inotropic agents.

1.1 Systolic function

The performance of the heart is governed by three principal factors :

1. Preload : the load on the myocardial fibers just prior to contraction, i.e. the amount of blood in the ventricle at the end of diastole.
2. Afterload : the external factors that oppose the shortening of muscle fibers, i.e. arterial impedance
3. Contractile or inotropic state of the myocardium

The first two determinants can be relatively easily measured or evaluated, but assessing contractile state is far more difficult. An index of contractility must assess the capacity of the heart to perform work. Moreover, since changes in loading almost always accompany alterations in the inotropic state any index intended to reflect contractility must be load independent.

1.2 Diastolic function

During diastole the myocardium stops shortening and generating force and relaxes. This results in a ventricular pressure decline at constant volume (isovolumic relaxation), followed by chamber filling, which occurs with increasing pressures. The diastolic function is characterized by the myocardium active relaxation properties (calcium recall and sequestration, crossbridge detachment, ATP metabolism...) and its passive stiffness (viscoelastic properties of the myocardium). A decrease in ventricular relaxation or increase in ventricular stiffness, reduce the capacities of the ventricular chamber to receive an adequate amount of blood during the diastolic filling phase, and can lead to diastolic heart failure.

The diastolic function can be evaluated by measurements of the ventricular pressure decline and filling (onset, rate, and extent) reflecting relaxation properties, as well as the relationship between pressure and volume during diastole which characterizes stiffness. Although some measurements mostly reflect the active relaxation and others the passive stiffness, they are closely related (i.e. processes that affect relaxation also alter stiffness and vice versa).

Even though relaxation is considered a diastolic process, it has a complex interaction with systolic events. This interdependence can alter the measurement and interpretation of active relaxation. For instance, the time of onset of active relaxation can alter systolic process but is also affected by the duration of contraction. It also influences the rate and extent of relaxation which additionally to being load dependent, would thus be affected by the duration of systole [10].

1.3 Overview of the Pressure-Volume Loop

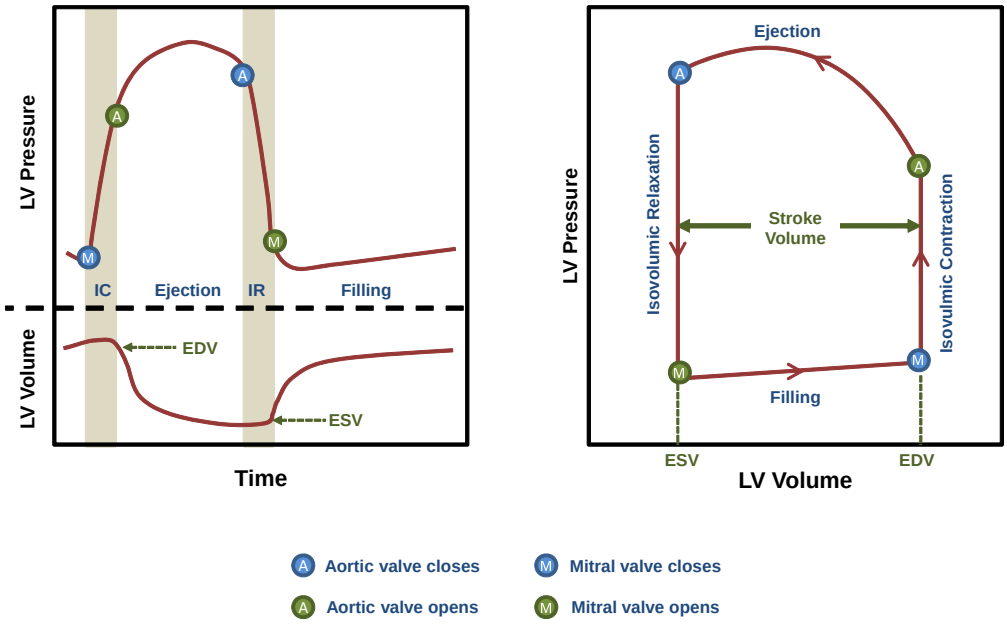

Figure 1 – The Pressure-Volume loop

The PV loop (figure 1) plots the left ventricle pressure versus the ventricle volume. Proceeding anticlockwise, the loop traces the chain of events of the cardiac cycle. Systole is represented in the right and upper boundaries of the loop, while diastole is included in the left and bottom boundaries. At the

bottom right corner of the loop is the mitral valve closure point, it occurs at end diastole when the pressure in the left ventricle exceeds that of the atrium. It is hereby referred to as the end diastolic point with coordinates (EDV, EDP). From that point, the isovolumic contraction starts, where the pressure in the LV increases at a constant volume, until the LV pressure exceeds that of the aorta causing the aortic valve to open. Once the aortic valve is open ejection starts. The pressure continues to increase while the chamber volume decreases as the blood is ejected into the aorta, this is known as rapid ejection. Once the peak systolic pressure is attained, slow ejection starts as pressure and volume both decrease. This continues until LV pressure becomes smaller than the aortic pressure causing the aortic valve to close. This point of the cycle is hereby referred to as end-systolic point with coordinates (ESV, ESP).The diastolic relaxation now begins. First the ventricle relaxes in an isovolumic manner, decreasing pressure rapidly at a constant volume, until the opening of the mitral valve when LVP becomes smaller than the atrium pressure. The blood now flows rapidly into the ventricle as it completes its relaxation, this is known as the rapid filling phase. The LVP then begins to increase while the volume increases as blood continues to flow in during the remainder of diastole, i.e. the slow filling phase (diastasis) and the atrial systole, until the mitral valve closes.

2 Experimental Protocol

The experimental measurements were acquired in collaboration with Emmanuel Durand (Univ. Paris Sud, CNRS, UMR8081), Ludovic de Rochefort (Univ. Paris Sud, CNRS, UMR8081), Younes Boudjemline (Univ Paris 05,Hôpital Necker-Enfants malades, AP HP) , and Elie Mousseaux.(Univ Paris 05,NSERM, U678)

2.1 Animal Preparation

Two female sheep were used in this study. An intervention on the first sheep was performed to compare the optical pressure sensor measurements against the Millar standard probes. A subsequent intervention on another sheep allowed simultaneous pressure and volume measurements. The ewes were placed in a sitting position to induce reflex akinesia then anesthetized with a slow injection of 1 g of diluted thiopental. Tracheal tube was inserted and forced ventilation was started with a concentration of 1.5-2% isoflurane to maintain anesthesia. To prevent clotting, acetylsalicylic acid (0.5 g) and heparin (3000 IU) were injected intravenously. The carotid artery was catheterized and a vascular dilator was inserted under X-ray monitoring. The animals received humane care in compliance with the standards of the European Convention on Animal Care. The study was approved by a local institutional ethics committee (INRA, Paris, France). Qualified personnel supervised the procedures and adequate anesthesia was used to minimize unnecessary pain.

2.2 In vivo pressure measurements

An optical pressure sensor probe (model OPP-M, Opsens, Quebec, Canada) based on the white-light polarization interferometry technique was used. The probe tip, 0.4 mm in diameter and 0.5 mm in length, attached to a 10 m long optical fiber directly transduces pressure into an optical signal which is then sampled at 1kHz. This device is fully MRI compatible, and immune to radio-frequency effects. The sensor is linear, with a total error of 2 mmHg and a temperature sensitivity of 0.2 mmHg/℃. Furthermore, each probe has two specific constant calibration factors.The nude fiber was sheathed into a non-magnetic 4F catheter (C4F100D, Balt extrusion, Montmorency, France) 1 m in length. The

sensor was positioned 5 mm before the catheter tip, facing a slot that had been manually cut in the catheter wall to ensure pressure transmission. The fiber was then glued into the catheter through another slot 5 mm above. A null point was set prior to inserting the sensor inside the sheep by zeroing the measurement at atmospheric pressure.

The validation of the optical probe against a reference pressure transducer (Millar, Houston, USA) was performed during an aortic intervention that served wider purposes than those stated in the present report. Guided by X-ray, the OpSens pressure sensor and the Millar catheter were introduced in the sheep's aorta via the carotid artery. While at the same position in the aortic flow, pressure signals were recorded simultaneously by both sensors. The animal ventilation was stopped for 20 seconds in order to acquire a stable signal with no respiration modulation. Figure 2 shows two 20 second extracts of the recorded signals, one while the ventilation was off and another, almost 2 minutes later during normal ventilation. Bland-Altman tests showed that the 95% confidence interval for the limit of agreement is of ± 2 mmHg when ventilation was stopped and ± 2.2 mmHg with ventilation. The Opsens offset was corrected such that the mean error would be zero. Figure 3a shows the extracted average cycles of both Opsens and Millar with no ventilation. A Bland-Altman test (figure 3b) performed on these cycles resulted in a 95% agreement limit of $[-1, +1.1]$mmHg, and showed that 99% of measurement differences lie within ± 1.6 mmHg. Figure 4 shows an example of simultaneous measurements of aortic and LV pressure.

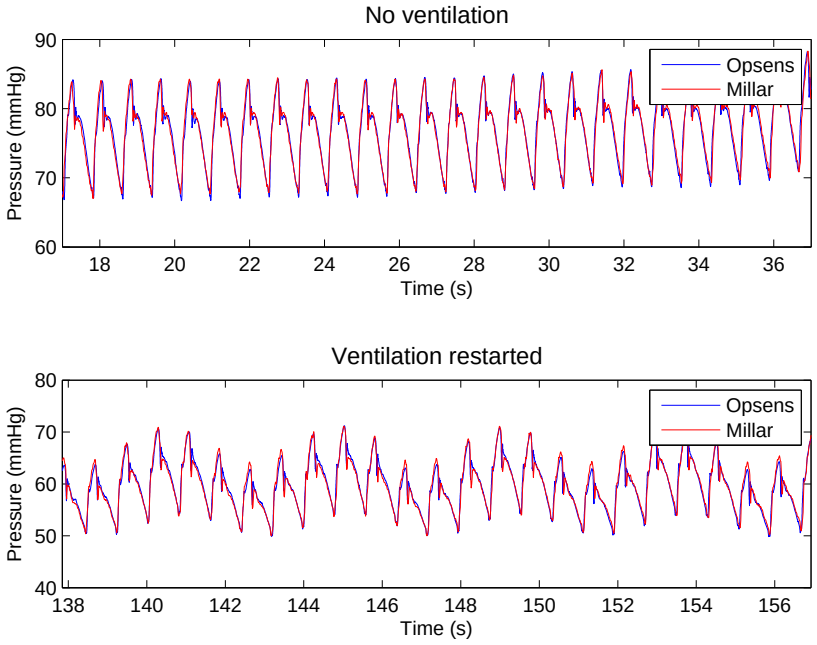

Figure 2 – Pressure signals recorded using OpSens vs those obtained by the Millar, with and without ventilation, where the OpSens offset had been corrected.

2.3 Simultaneous in vivo pressure and volume measurements

Pressure measurements with the optical probes were conducted simultaneously with MRI acquisitions in another female sheep (60 kg). After four acquisitions at a baseline condition (heart rate ranging between 78 and 83 bpm), the sheep was infused dobutamine at a rate of 5 µg/kg/min. Heart

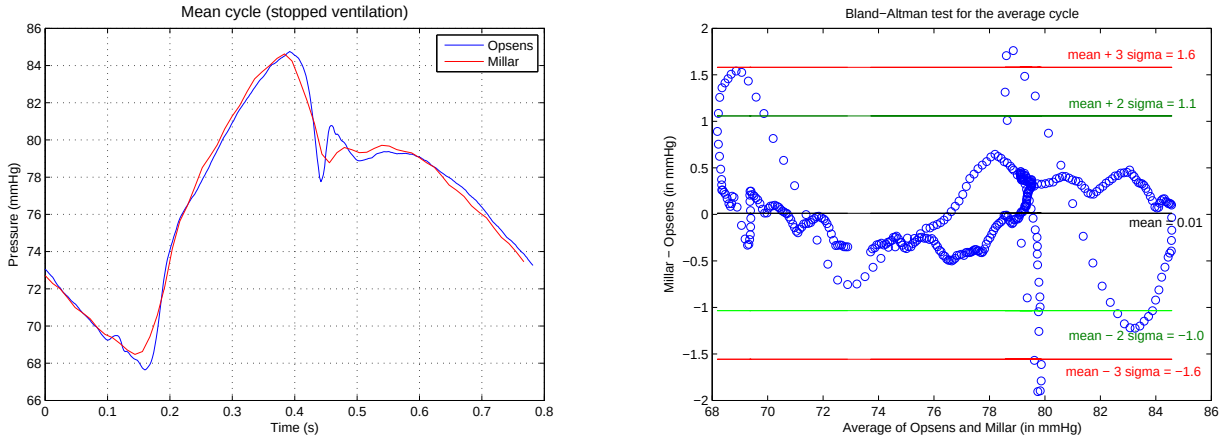

(a) Opsens and Millar average cycles

(b) Bland-Altman test on the average cycles

Figure 3 – Average cycle comparison

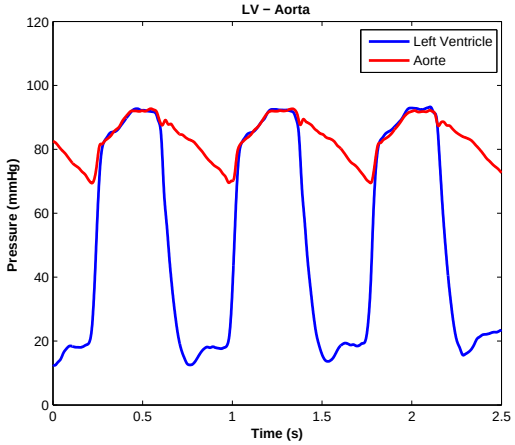

Figure 4 – Pressures in the LV and the Aorta

rate increased to 145-150 bpm and three acquisitions were performed. Dobutamine rate was then decreased to 2.5 µg/kg/min (heart rate decreased to 125-131 bpm) and a last acquisition was performed before waking the animal up. The whole MR procedure lasted 2 hours and 20 minutes.

2.4 Magnetic resonance imaging acquisitions

Cardiac imaging was performed with a 1.5 T MR scanner (Philips Medical Systems, Achieva) with a 5-element SENSE cardiac array coil and ECG triggering. After calibration and scouting sequences, true FISP gated cine images ("balanced TFE") were acquired in 12 sequential 8-mm short-axis slices (2 mm interslice gap) from the apex to the atrial-ventricular ring, for 30 cardiac phases (TE/TR= 1.7ms/3.4ms, flip angle of 60°, field of view=320 x 240 mm^2, matrix=256 x 192, voxel size 1.25mm, echo train length of 10, readout bandwidth 1042 Hz). Mechanical ventilation was continued during the MRI acquisition procedures without respiratory synchronization. Other sequences were also acquired for other purposes, not mentioned here.

3 Pressure-Volume loop Computation

For each slice, the LV was delineated (figure 5) and its area was computed then multiplied by the slice thickness to derive an elementary volume. These slice volumes were then added up to define the total LV volume. This was performed for all cardiac phases, and an LV volume evolution in time was obtained.

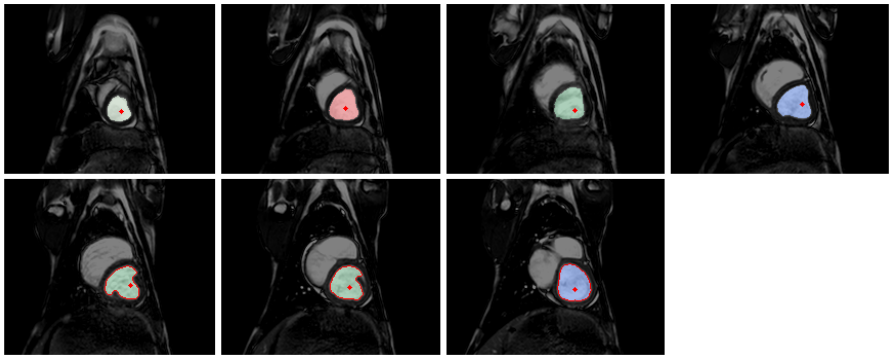

Figure 5 – Slices area delineation for a given cardiac phase

During each of the imaging sessions the ventricular pressure was recorded continuously. Since we only have one volume curve reflecting a somewhat average volume evolution during the image acquisition, an average pressure cycle was derived for the loop computation. Figure 6 summarizes the cycle calculation. To delimit a heart cycle, pressure peaks were considered to be the end points of a pressure period. By applying a double threshold on the pressure signal, we delimited individual windows each containing a pressure peak. Afterward the local maximum is identified inside each window, thus defining a cycle end point. Once all peaks are determined, individual periods T_i are computed, and cycles are extracted between $t_{peak,i} - \frac{T_i}{2}$ and $t_{peak,i} + \frac{T_i}{2}$. These cycles are then averaged to yield a mean pressure curve. The volume and pressure curves were then associated by assuming that maximum volume is attained with maximum $\frac{dP}{dt}$. An example of the computed pressure and volume curves is given in figure 7.

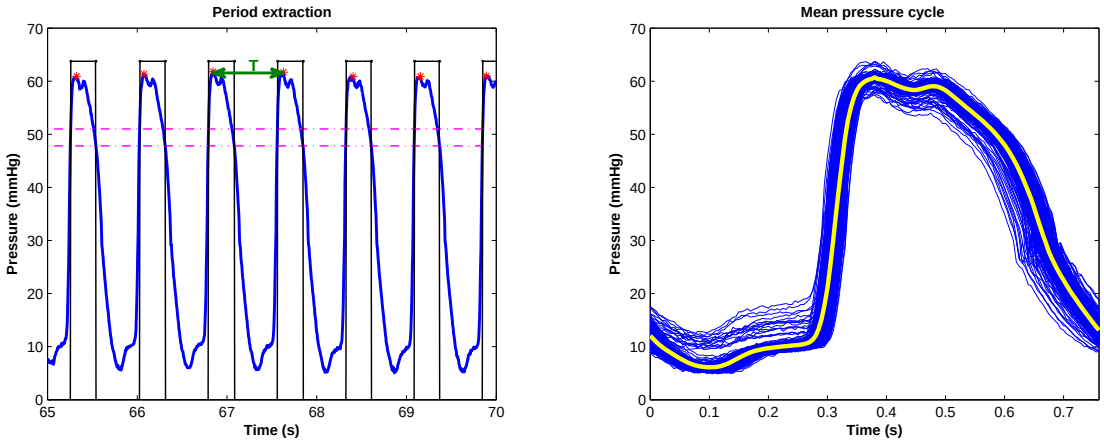

(a) Extraction of heart cycle

(b) Averaging over extracted periods

Figure 6 – Mean pressure cycle computation

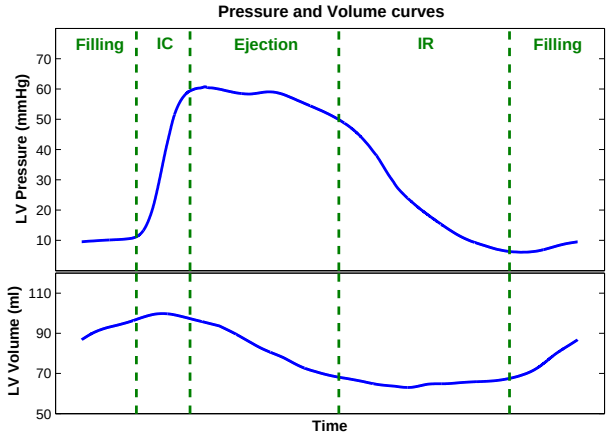

Figure 7 – Associated LV pressure and volume curves

4 Pressure-Volume Analysis

4.1 Stroke volume (SV), Ejection Fraction (EF) and Cardiac Output (CO)

The most straightforward indicators of the pump function of the heart are the stroke volume, ejection fraction and cardiac output. The stroke volume defines the amount of blood ejected in one heart cycle. It is computed as $SV = EDV - ESV$. The ratio of the stroke volume to the total blood volume present in the ventricle at end systole (EDV) yields the ejection fraction $EF = SV/EDV$. The cardiac output defines the quantity of blood pumped by the heart per time unit and is expressed as $CO = SV * HR$, where HR stands for the heart rate. Though intuitive and simple, these parameters are not sufficient for the evaluation of the cardiac function. For instance, they can't be relied on for detecting heart failure and cardiac dysfunction [1, 2]. Moreover, given that they depend on load (EDV, arterial elastance, ...), they cannot solely characterize contractility and cardiac response to inotropic agents.

4.2 End-Diastolic Pressure-Volume Relationship (EDPVR)

During the diastolic filling phase, the myocardium behaves as a passive elastic body that is being stretched, and thus in order to resist deformation, it develops a growing tension as its length increases with incoming blood. The pressure volume relationship, during this phase, known as the EDPVR, is generally exponential and depends on the elastic properties of the myocardium, the wall thickness and the ventricle's equilibrium volume V_0 [18]. V_0 being defined as the intercept of the EDPVR with the volume axis, it's the volume that the ventricle exhibits when subjected to no transmural pressure (see figure 8).

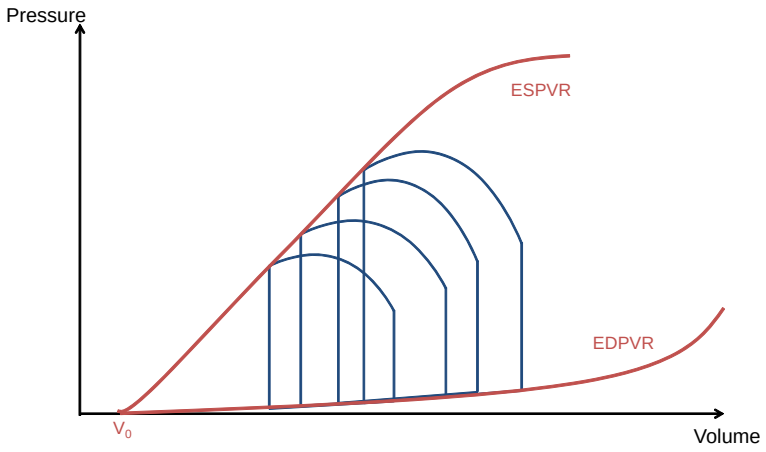

Figure 8 – ESPVR and EDPVR

At any given instant of the EDPVR, the ventricle's stiffness modulus $E = \frac{\partial P}{\partial V}$ is given by the slope of the tangent to the curve at that point. We can also reason in terms of compliance and compute $C = \frac{\partial V}{\partial P}$ as the slope reciprocal. Given the exponential nature of the EDPVR, the ratio of pressure to volume increases as the ventricle continues to fill, thus leading to a decreasing compliance. For small volumes the ventricle is very compliant, but as the chamber extends it becomes more and more stiff, as for most biological tissues. The overall chamber stiffness is defined by the myocardium stiffness as well as the ventricle mass and its mass to volume ratio [10].

It's important to note that the myocardium is not a purely elastic material but also presents viscous behavior, meaning that the developed pressure, not only depends on the volume extension, but also on the extension rate (i.e. the filling rate). This dependence implies that for faster filling rates, the pressures are more elevated for a given volume, and the EDPVR would become steeper. During diastasis, given that the filling rate is very slow, viscous forces can be ignored, nevertheless they do contribute to the myocardial response during rapid filling and atrial systole when rates are high. The viscoelastic effects are however more prominent in atrial systole, than rapid filling when they are overshadowed by relaxation effects [19].

The EDPVR is independent of the contractility state. When the inotropic state is enhanced (or decreased), the diastolic filling portion of the PV loop would remain on this curve while sliding towards the left (or the right) [20, 21]. This of course leads to compliance alterations in response to inotropic changes. For instance, decreased contractility would lead to higher ESV, causing a filling at a steeper portion of the EDPVR, and thus higher stiffness.

In this study the EDPVR is fit with $P = \alpha\left(e^{\beta(V-V_0)} - 1\right)$, and the compliance is computed using the slope of the EDPVR during the slow filling phase, thus reflecting purely elastic properties of the ventricle.

4.3 End-Systolic Pressure-Volume Relationship (ESPVR)

The ESPVR is constructed from a series of PV loops with different ventricular filling volumes. It is formed by the line connecting the end-systolic points of all PV loops, as shown in figure 8. For a given contractile state the PV loops are confined beneath the ESPVR curve. This relation can be approximated as linear in the physiological range and characterized by its slope, the end-systolic elastance E_{es}, which reflects the ventricular contractility state [22, 23] and a volume intercept at a given pressure that defines its position in the PV plane. Analogous to the force length relationship of a spring, the ESPVR line can be used for assessing mechanical potential energy and ventricular efficiency, as will be discussed in a further section.

4.4 End-systolic elastance E_{es}

Suga *et al.* [24] viewed the ventricle as having a time varying elastance $E(t) = \frac{P(t)}{V(t)-V_0}$, V_0 being the intercept of the ESPVR with the volume axis (the theoretic volume for which no pressure is developed). The slope of the ESPVR gives, thus, a measure of the ventricular elastance when the contractile forces in the ventricle are at their peak. E_{es} is a good indicator of the ventricular contractility and systolic function, because unlike cardiac output, stroke work and dP/dt, the maximum elastance is independent of preload after-load and heart rate [11, 12]. Positive inotropic interventions would increase E_{es} and shift the ESPVR to the left, while depressors of the cardiac function would decrease E_{es} shifting ESPVR to the right, nevertheless the volume axis intercept V_0 would not significantly change [25, 20]. Even though repeated E_{es} and V_0 measurements in the intact cardiovascular system show statistically significant variability because of the autonomic nervous system reflexes, they are still considered valid indexes of the inotropic state [25].

ESPVR and E_{es} estimation The ESPVR is usually obtained by computing several PV loops while gradually decreasing preload, using a balloon occlusion of the vena cava, for example. This procedure's invasive nature, limiting clinical applications, has motivated several authors to propose methods for computing the ESPVR from a single PV loop. Takeuchi *et al.* [26] simulated end-systolic

isovolumic pressure by cosine fitting of the pressure curve, to locate a theoretical P_{iso} that would be attained if ejection did not take place. The E_{es} is then computed as the slope of the line connecting the point defined by (EDV, P_{max}) to the end-systolic point on the PV loop. Other authors relied on a time-varying elastance model. Senzaki *et al.* [27] calculated the volume axis intercept of the elastance curve then defined the ESPVR by connecting this point with the end-systolic point of loop. Shishido *et al.* [28] refuted some assumptions made by Senzaki *et al.* and focused on the shape of the curve and performed a bi-linear fitting to derive E_{es}. Chen *et al.* [29] later proposed a simplification of this model.

Although these single-beat estimation methods were tested and validated on humans and other species, some authors [30] have emitted doubts about their accuracy and their capabilities to assess ventricular contractility. Recently Brinke *et al.* [11] using Takeuchi*'s* technique with a modified fitting scheme (fifth order polynomial instead of a cosine), showed that a good estimation of intercept volumes can be achieved. They argued that even though the single beat estimation might underestimate E_{es} and does not agree closely with the vena cava occlusion technique estimation, it is still a reasonable approach given its experimental advantages.

Since the single beat methods use load dependent elements such as dP/dt and EDV, it is more valid to view them as load dependent approximations of the load-independent elastance [30].

In this study we estimated the ESPVR following the method proposed by Brinke *et al.* [11]. We computed a maximum isovolumic pressure P_{iso} by using a spline interpolant fitting scheme to fit the left ventricle pressure curve. We started after end diastole and excluded from the fitting the pressure data points that lie after dP/dt_{max} and before dP/dt_{min} and those after the point where dP/dt increased above 15% of dP/dt_{min}. Figure 9 summarizes this procedure.

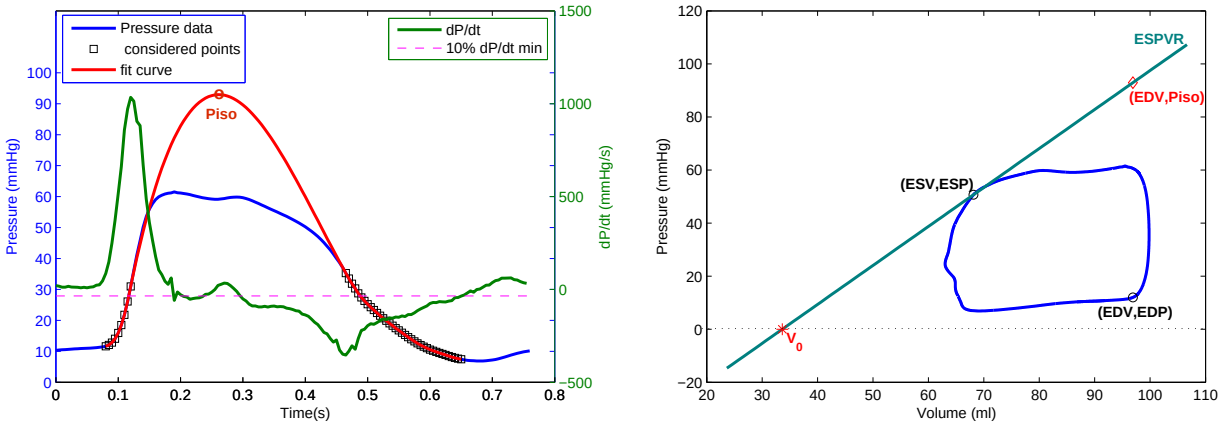

(a) Estimation of P_{iso} by fitting the pressure curve

(b) ESPVR in the PV plane

Figure 9 – Single-beat ESPVR estimation

4.5 Time to end systole (T_{es})

Contractility can also be characterized by the duration of systole. Based on the time varying elastance model, this time can be viewed as the time necessary for $E(t)$ to reach E_{es} starting from the onset of systole (end diastole). T_{es} is load independent and shortens with the enhancement of contractility state [24, 4]. Nonetheless, unlike E_{es}, T_{es} varies with heart rate [24], thus limiting its use as an absolute index of inotropy.

4.6 Maximal first derivative of pressure (dP/dt_{max})

The maximum rate of change (dP/dt_{max}) occurs early during isovolumic contraction, it is sensitive to inotropic state and thus correlate with cardiac contractility. Nonetheless, its load dependence [3, 4, 5] makes it a poor contractility index.

To negate preload dependency, rather than considering dP/dt_{max}, the relationship of this value to EDV can be computed by varying preload conditions. This relationship is linear and its slope provides a preload-independent contractility index which is proportional to the ratio of the E_{es} to T_{es} [9]. Based on the time varying elastance model, Little [9] gives the dp/dt_{max} as $\frac{dP}{dt}_{max} = k\frac{E_{es}}{T_{es}}(V_{ED} - V_0)$ where V_0 is the volume intercept of the ESPVR (this means that this relationship and the ESPVR have the same volume axis intercept) . Since both E_{es} and T_{es} are load- independent, the slope is also load independent. Moreover, we know that E_{es} increases with enhanced inotropic state, while T_{es}decreases, hence the slope of the dp/dt_{max}vs EDV relation would be highly sensitive to inotropic changes and will increase in response to positive inotropic stimuli [9, 4]. Even though this index is more sensitive to inotropic changes than E_{es}, like T_{es}, it depends on heart rate. It was also shown to be statistically variable at constant inotropic state [31].

As for its afterload dependency, Little [9] argued that it is less sensitive than the ESPVR to alterations of the arterial characteristics. He showed that the slope of the dP/dt_{max}vs EDV relation remains somewhat unchanged in response to increase in aortic pressure produced by vasoconstriction, while the ESPVR is shifted to the left, and its slope is slightly decreased. On the other hand, Mason *et al.* [5] discussed that since dP/dt usually peaks at the opening of the semilunar valves, it is deeply affected by the arterial diastolic pressure. They stipulated that the rate of pressure change is independent of afterload, only when dP/dt_{max} occurs before the onset of ejection (i.e. when diastolic pressure is very high).

Kass *et al.* found that in the presence of both preload and afterload alterations, E_{es} was relatively less affected than dP/dt_{max}vs EDV . So, despite E_{es}'s lesser sensitivity to inotropic change, its minimal dependence on both types of load alterations, coupled with its adequate characterization of contractility, make it somewhat more advantageous than dP/dt_{max} vs EDV [4].

4.7 Minimal first derivative of pressure (dP/dt_{min})

The peak decline of pressure (dP/dt_{min}) occurs early in diastole, usually shortly after the aortic valve closure [7] and quantifies isovolumic relaxation. It can't however be qualified as an intrinsic relaxation index since it is preload-dependant [6] as well as afterload-dependant [7] (alterations in afterload result in changes in peak aortic pressure and/or the timing of the aortic valve closure). Moreover, given the existing interaction between the relaxation process and systolic events, the measure of dP/dt_{min} cannot strictly describe the relaxation process, its value could reflect some systolic properties. For example [6] showed alterations of dP/dt_{min} in response to inotropic stimuli.

4.8 Isovolumic relaxation constant (τ)

During isovolumic relaxation, the pressure decay from the time of dP/dt_{min} to the time where pressure reaches EDP level, is exponential such that $P(t) = P_{dP/dt_{min}} * e^{-t/\tau}$and can therefore be characterized by a time constant τ [7] . τ is the time that it takes for the pressure to fall by approximately two thirds of its initial value. When isovolumic relaxation is slowed, τ is prolonged. Although afterload dependent, τ was shown to be preload-independent [8]. Usually it is evaluated over a range of afterloads and plotted against EDV [10].

Even if it's not an ideal index , τ is widely used for relaxation quantification.

In this study, τ is computed using an exponential fit of the pressure points lying between dP/dt_{min} and the start of the filling phase (when dP/dt increased above 15% of dP/dt_{min}) as shown in figure 10 .

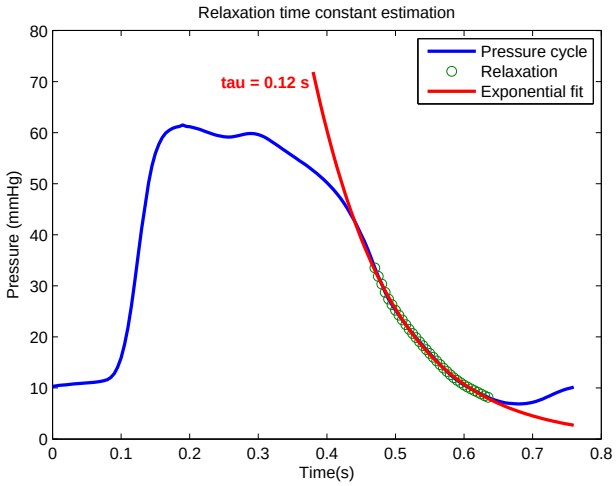

Figure 10 – Relaxation time constant estimation

4.9 Effective Arterial Elastance (Ea)

The arterial system, as afterload, can be assessed from the PV loop, and, like the ventricle chamber it can be characterized by its elastance E_a. The arterial elastance is determined by the pressure in the ventricle at end systole, and the amount of blood that the ventricle ejected into the arterial system. In fact, as the aortic valve closes, the pressure in the aorta is somewhat equal to ESP and it contains the volume SV, such that its elastance can be computed as $E_a = ESP/SV$. It can be represented on the PV loop diagram as the line connecting the end systolic coordinates and the EDV point on the volume axis as shown in figure 11. This allows the representation of the interaction between contractility and afterload in the same diagram, where both are described in equivalent terms. For instance, for a given contractility state (E_{es}) and a given preload (EDV), when E_a increases (stiffer arteries), the SV and EF decrease, and the ESP increases, reflecting the effect of enhanced afterload.

Indeed this is not a measure of the elastance of the whole arterial tree, and thus is referred to as the effective arterial elastance. Studies have shown the importance of E_a as a descriptor of the vascular load and its impact on cardiac performance [13, 14], indicating that the ratio E_a/E_{es} quantifies the coupling between the ventricle and arterial system and governs ventriculoarterial matching. This coupling determines the stroke volume, and defines the ventricle's energy utilization efficiency to achieve that SV, as will be discussed subsequently.

4.10 Stroke Work (SW) and Preload Recruitable Stroke Work (PRSW)

The area inside the PV loop has the units of energy (pressure multiplied by volume) and characterizes the external mechanical work achieved by the heart to eject the SV, this is called the stroke work. The mechanical energy of contraction produced by the ventricle, i.e. the SW, is stored as hydraulic

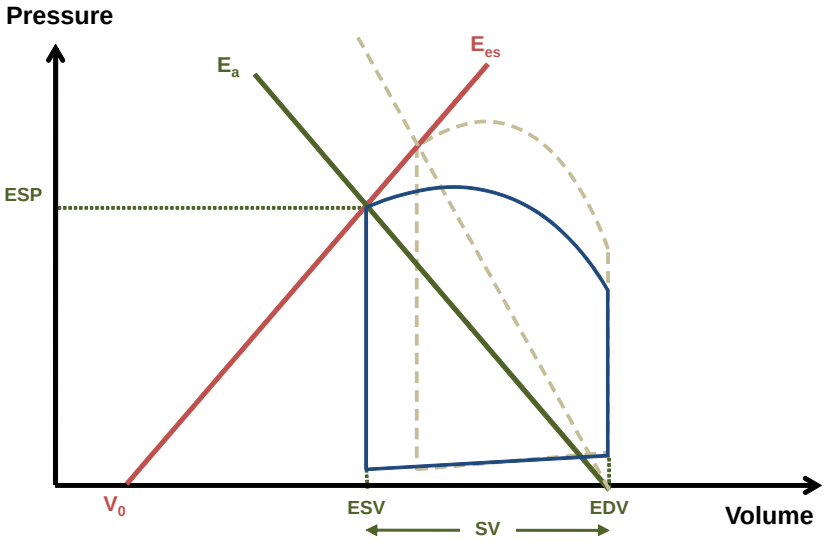

Figure 11 – Effective arterial elastance

energy in the ejected blood and thus transferred to the arterial system. As in any physical system, the maximal transfer of energy from the source to the load is achieved when the input impedance of the load is equal to the output impedance of the source, the source and the load are said to be matched. Similarly, the energy transfer from one elastic chamber to another is maximal when they both have the same elastance [32]. Accordingly, maximal SW would occur when $E_a = E_{es}$.

The SW varies very slightly with afterload but is very sensitive to preload [4] , and thus the study of the relationship between the EDV and the SW has been judged more suitable. This relationship is called the preload recruitable stroke work (PRSW). It is a linear relationship [33] which slope reflects the inotropic state. Slope and elevation increase with positive inotropic stimuli whereas they decrease in response to negative inotropic agents [20]. It was also shown to be insensitive to afterload over the physiological range, and thus qualifies as a contractility index, although it might depend on cardiac geometry and heart rate [33].

Unlike the ESPVR which takes into account end systolic information only, the PRSW integrates data from the whole cycle. Little *et al.* [31] showed that the PRSW is less sensitive than the ESPVR to afterload, its slope is more reproducible (less variable for a given inotropic state) than E_{es}, and that of dP/dt_{max} vs EDV . Its volume intercept is much more stable than that of ESPVR, and dP/dt_{max} vs EDV, and it remains unchanged in response to inotropic stimuli [31]. Nonetheless, the PRSW is less sensitive to inotropic changes than E_{es} and dP/dt_{max} vs EDV [31].

In this study, since preload conditions variation was not performed, the PRSW could not be computed. A method to estimate the slope of PRSW from a single beat was proposed by Mohanraj *et al.* [34], however their method did not exclude prior preload variation experiments. For their estimations they computed an empirical constant from a set of VCO experiments, which they used for the slope estimation of another group of the same species.

4.11 Potential Energy (PE)

Potential energy, is the mechanical energy that is available in the ventricle at end systole. It is the energy that was not converted into external work because the aortic valve had closed, and will be dissipated during relaxation. This energy can potentially produce external mechanical work if there were no afterload.

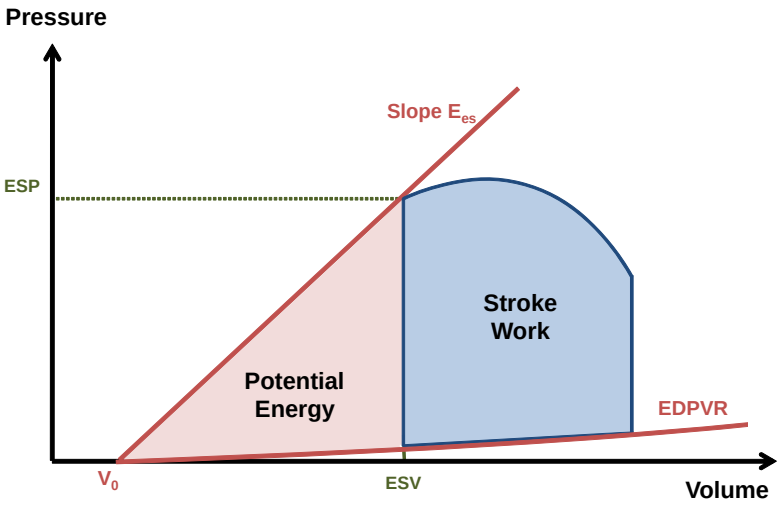

Figure 12 – Mechanical energy

At end systole, the ventricle has a certain pressure ESP for a given volume ESV, it presents a stiffness E_{es}, and, like a stretched Hookean spring, stores energy that depends solely on its elongation and elastance. We know that the potential energy of a Hookean spring that was stretched from its rest length L_0 to L_s, is given by $\frac{1}{2}k(L_s - L_0)^2$ where k is the spring elastance. Similarly, we can say that the potential energy that the ventricle holds at end systole would be given by $\frac{1}{2}E_{es}(ESV - V_0)^2$, this represents the area under the ESPVR spanning from V_0 to ESV. Note that the part of this area that lies beneath EDPVR represents energy that is not actively supplied, it results from passive stretching due to the incoming blood, and the PE release during relaxation can never situate the ventricle under this curve. Thus, this area portion must not be included for the potential energy calculation. Therefore the PE is represented by the area of the triangle between the point of end systole on the PV loop, V_0 and the ESV intercept on the EDPVR, as shown in figure 12. The PE thus depends on contractility (E_{es}), passive filling behavior, and afterload (E_a) which defines end systolic pressure and volume. Any situation that alters any of these elements, will affect the potential energy.

4.12 Pressure Volume Area (PVA)

The total mechanical energy of a ventricular beat is known as the pressure volume area and is equal to the sum of potential energy and stroke work, $PVA = PE + SW$.

PVA characterizes the ventricle's oxygen consumption.There is a linear correlation between PVA and oxygen consumption, V_{O_2} increases as PVA increases. Furthermore, the slope of this linear relation is independent of contractility, but shifts up (or down) as contractility increases (or decreases) [12]. PVA also contains information on crossbridge behavior in a beating heart, and combined with E_{es} it can be used to assess the total amount of Ca^{2+} released and removed for contraction [12].

4.13 Mechanical efficiency

Like any other system, the mechanical performance of the ventricle is defined by its ability to convert metabolic energy into external mechanical work. In other words, it is the ratio of SW (the effective energy output) to the oxygen consumption (total energy consumption). This ratio is a function of ventricular loading and contractile state.

The mechanical efficiency can be decomposed in two stages :

- ▷ The efficiency of energy transfer from oxygen to total mechanical energy PVA/V_{O_2}. For a given PVA, this ratio increases with depression of contractility and with afterload [35]. Conversely, when contractility is enhanced, the V_{O_2}vs PVA relation is shifted upwards, more oxygen is consumed for the same PVA, and thus oxygen conversion efficiency is decreased.
- ▷ The efficiency of energy transfer from the ventricle to the arterial system SW/PVA, called cardiac work efficiency (CWE). This is the portion of the total generated energy that is actually converted into external work. SW/PVA is reciprocally related to $\frac{E_a}{E_{es}}$ [35] which determines the position of the end-systolic coordinate, thus defining the relative contributions of SW and PE to the PVA. The cardiac work efficiency increases with contractility enhancement, and decreases with afterload increase [36]. Studies have shown that the CWE is maximal when $\frac{E_a}{E_{es}} = 0.5$ [37, 38].

Given the opposite effects of inotropy and afterload on both efficiency indexes, their changes could compensate when the inotropic state or afterload are altered, leading thus to no changes in the total mechanical efficiency [35].

Optimal working point To fulfill its pumping function, the heart must transfer enough energy to the arterial system to ensure adequate flow and perfusion pressure while remaining as efficient as possible. The cardiovascular system, thus matches the ventricular and arterial properties so that ventriculoarterial coupling would best achieve that function. As mentioned, CWE is optimized when the arterial elastance is nearly one half the end systolic elastance, while on the other hand, SW is optimized when both elanstances are equal. It has been shown that the normal heart at rest operates at neither maximal CWE ($E_a/E_{es} = 0.5$) nor maximal SW ($E_a = E_{es}$), but in fact finds an optimal working point between the two, which is actually closer to maximal efficiency [37, 38]. SW might however be favored at the expense of CWE in some cases of mild cardiac dysfunction [38].

5 Results

Pressure-volume loops were computed for all measurements covering four contractility states. Overall we obtained 9 PV loops : 4 for baseline, 1 with Dobutamine 2.5, 3 with Dobutamine 5 and 1 with Esmolol.

5.1 Pressure offset correction

Even though the dynamics of the pressure measurements performed here were shown to be accurate, the used pressure sensors present an offset that drifts throughout the experiment, thus introducing an unknown pressure shift between the measurements. This variable drift can exceed 2 mmHg/hour. In order to be able to compare the obtained loops and the extracted parameters, a correction is necessary to bring the pressure cycles to a common reference. To eliminate these relative offsets we relied on theoretical fact that the filling parts of all measured PV loops should lie on the same EDPVR. Hence, we computed that relation for one of the baseline loops (we chose the fourth) and then shifted the pressure cycles of the rest of the loops so that they would be supported by the estimated EDPVR. Of course this does not eliminate the “absolute” pressure offset that is added to

the reference pressure measurement, but at least all loops now have that same offset and can be compared.

An attempt to estimate and correct the absolute offset can be made by considering the EDPVR and ESPVR intersection point. Theoretically these relationships should have the same zero axis intercept. Thus, we could assume that the absolute offset would be eliminated by shifting the reference baseline loop so that EDPVR and ESPVR intersect at zero pressure. Of course the same shift would afterward be applied to the rest of the loops. This procedure would, however, not guarantee the elimination of the real offset, in fact it depends greatly on the ESPVR estimation, which itself is not very accurate given that it's computed from a single beat. Besides given the instability of ESPVR and V_0 and their variability between repeated measurements [25], the chosen loop probably does not reflect the real V_0.

To sum up, the presented pressures here might not actually reflect the real ones, but present a residual offset that introduces errors in the calculations of some parameters, such as ESP, EDP, P_{max}, V_0,PE, and E_a. Other parameters such as E_{es} , C , and SW, are independent of the pressure offset and thus can be assumed accurate even if there's an unknown shift of the PV loop. Regardless of whether the offset is important or not, comparison between the considered contractility states remains valid, since the relative offsets are corrected and the absolute shift applies equally to all states. Further studies will focus on modeling the sensors behavior to enable measurement correction.

5.2 Baseline measurements

Figure 13 shows an example of a baseline loop and some of the extracted parameter values. The computed mean baseline parameters are compared to values obtained in other studies dealing with sheep [39, 40, 41, 42, 43, 44] in order to situate our calculations with respect to usual parameter values. Figure 14 shows a graphical representation of these values for rapid visual comparison. Some parameters such as E_{es} for example agree well with the literature range. Others, like the compliance and V_0, differ significantly from what is obtained by other authors. These differences can be explained by the fact that the sheep studied by those authors are a lot smaller (weighting around 40 kg) than the one used in our experiments (70 kg). Since the diastolic compliance decreases with the chamber size [45, 46], smaller animals with smaller hearts have less compliant ventricles. Moreover, smaller volumes mean that the PV loops are shifted to the left, thus the ESPVR axis intercept is also shifted to the left, thus explaining the smaller V_0.

5.3 Contractility states comparison

Figure 15 shows the experimental time line and heart rate evolution throughout the consecutive states. The instantaneous frequencies were computed, over the pressure recordings, as the inverse of the time interval separating two pressure peaks, as shown in figure 6a. HRincreases gradually after the Dobutamine administration starts, it stabilizes then decreases when the Dobutamine rate is diminished. A HR increase can be observed as we go from one rate to another, as the remaining Dobutamine might have been injected rapidly to evacuate the tubes for the next perfusion. Esmolol administration slows down the heart, and as soon as it is stopped, the heart starts recovering. Note that, the recorded recovery measurements did not last long enough to observe the HR going back to its normal value.

Of course, functional changes in response to the inotropic agents, go beyond the obvious HR variation. Not only did the pressure cycle period vary, but its shape was drastically altered. Figure 16

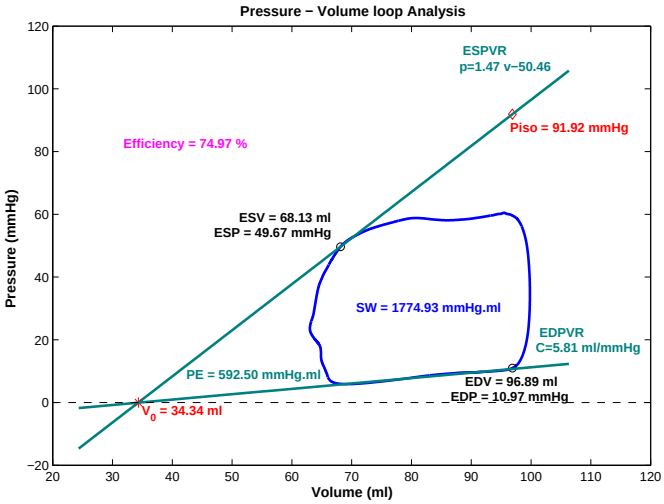

Figure 13 – Baseline parameter extraction example

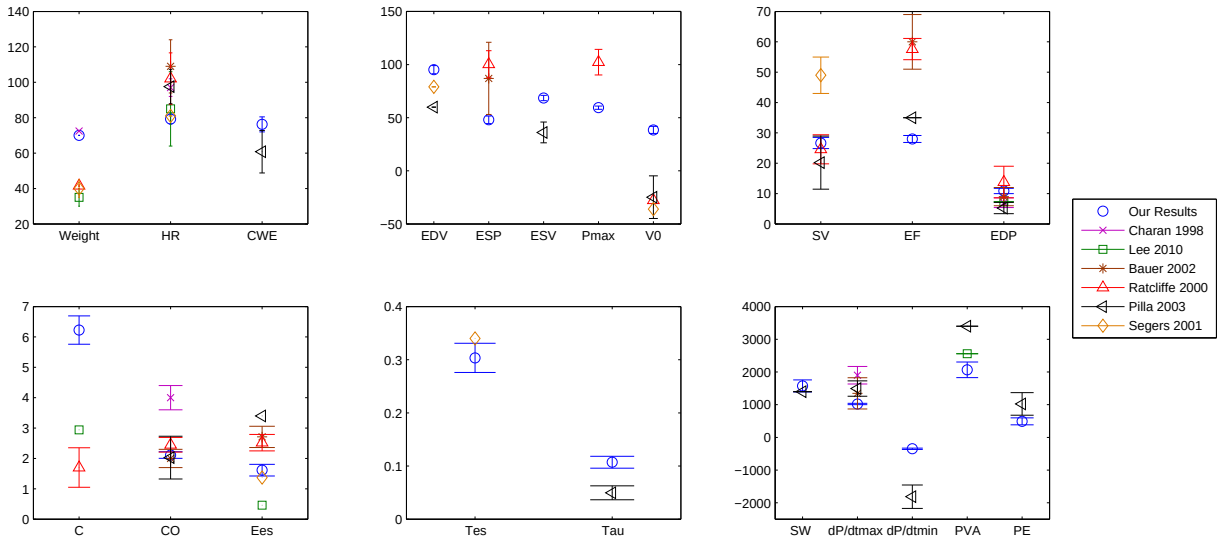

Figure 14 – Comparison with the literature

Charan *et al.* [39], Lee *et al.* [40] , Bauer *et al.* [41], Ratcliffe *et al.* [42], Pilla *et al.* [43], and Segers *et al.* [44].

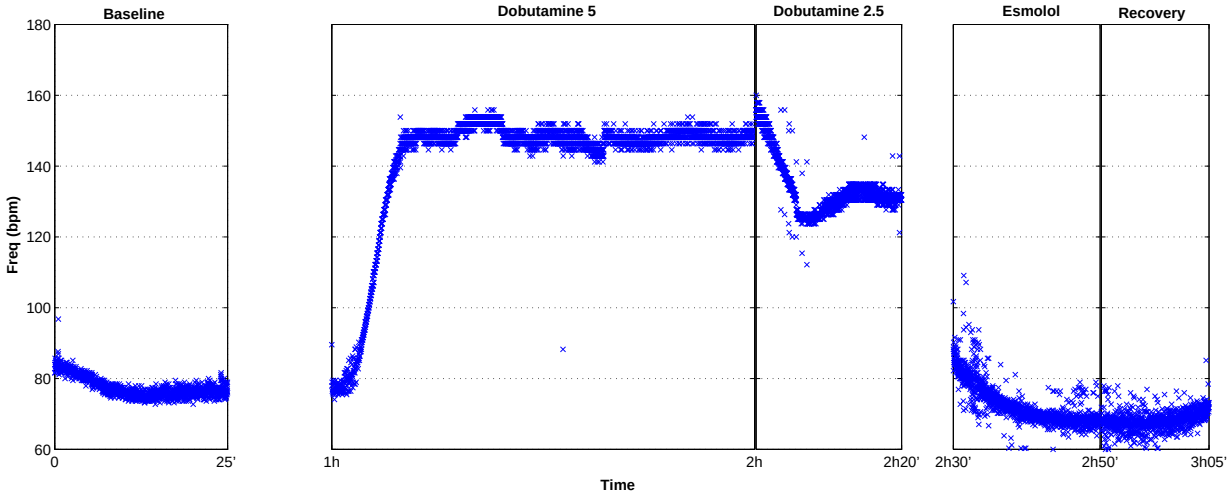

Figure 15 – Frequency evolution throughout the experiment

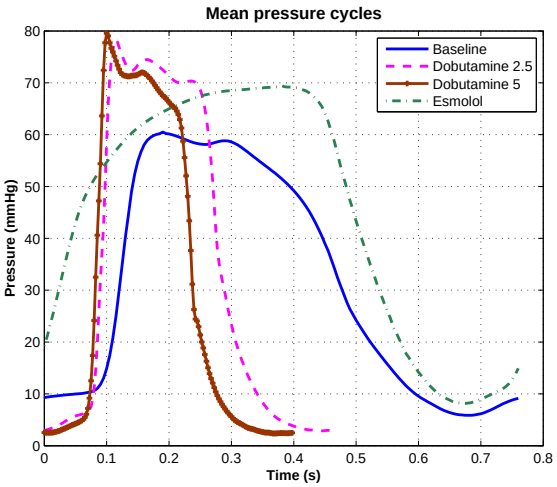

Figure 16 – Mean pressure cycles

shows mean pressure cycles, each representing an inotropic state. Contrarily to what would be expected, the amplitude of the pressure cycle during Esmolol, is higher than that of the baseline. This could be because the steady state under Esmolol was not reached. Esmolol was administered right after the Dobutamine, and the measurement time under this state was short.

		Esmolol	*Baseline*			*Dobutamine 2.5*	*Dobutamine 5*		
HR	(bmp)	*78.95*	*78.28*	$\pm$	*2.79*	*129.77*	*150.99*	$\pm$	*0*
EDV	(ml)	*99.92*	*95.22*	$\pm$	*3.82*	*69.25*	*62.31*	$\pm$	*4.60*
EDP	$(mmHg)$	*19.27*	*10.88*	$\pm$	*0.87*	*8.77*	*7.68*	$\pm$	*0.64*
ESV	(ml)	*77.68*	*68.55*	$\pm$	*2.49*	*43.86*	*41.72*	$\pm$	*4.54*
ESP	$(mmHg)$	*66.90*	*48.04*	$\pm$	*3.58*	*66.99*	*56.40*	$\pm$	*8.68*
SV	(ml)	*22.24*	*26.67*	$\pm$	*1.84*	*25.39*	*20.59*	$\pm$	*1.40*
EF	$(\%)$	*22.26*	*27.99*	$\pm$	*1.16*	*36.66*	*33.14*	$\pm$	*2.88*
CO	(l/min)	*1.75*	*2.11*	$\pm$	*0.10*	*3.29*	*3.10*	$\pm$	*0.21*
P_{max}	$(mmHg)$	*69.49*	*59.46*	$\pm$	*1.53*	*78.31*	*77.64*	$\pm$	*2.52*
C	$(ml/mmHg)$	*3.90*	*6.23*	$\pm$	*0.47*	*6.88*	*8.55*	$\pm$	*3.35*
E_{es}	$(mmHg/ml)$	*1.55*	*1.62*	$\pm$	*0.19*	*3.83*	*4.21*	$\pm$	*0.26*
V_0	(ml)	*34.64*	*38.49*	$\pm$	*3.36*	*26.35*	*28.26*	$\pm$	*6.59*
T_{es}	(s)	*0.43*	*0.30*	$\pm$	*0.03*	*0.18*	*0.15*	$\pm$	*0*
$\frac{dP}{dt}_{max}$	$(mmHg/s)$	*510.48*	*1020.64*	$\pm$	*20.24*	*3370.92*	*3556.28*	$\pm$	*232.13*
$\frac{dP}{dt}_{min}$	$(mmHg/s)$	*-491.60*	*-347.02*	$\pm$	*20.26*	*-1860.39*	*-2342.00*	$\pm$	*428.75*
τ	(s)	*0.10*	*0.11*	$\pm$	*0.01*	*0.04*	*0.03*	$\pm$	*0*
SW	$(mmHg.ml)$	*1301.16*	*1574.27*	$\pm$	*183.24*	*1939.42*	*1548.46*	$\pm$	*229.35*
PE	$(mmHg.ml)$	*1188.56*	*491.89*	$\pm$	*107.13*	*457.67*	*210.26*	$\pm$	*84.61*
PVA	$(mmHg.ml)$	*2489.73*	*2066.15*	$\pm$	*238.61*	*2397.10*	*1758.71*	$\pm$	*309.27*
CWE	$(\%)$	*52.26*	*76.26*	$\pm$	*4.23*	*80.91*	*88.38*	$\pm$	*3.24*
E_a	$(mmHg/ml)$	*3.01*	*1.81*	$\pm$	*0.18*	*2.64*	*2.74*	$\pm$	*0.37*
E_a/E_{es}		*1.94*	*1.12*	$\pm$	*0.11*	*0.69*	*0.65*	$\pm$	*0.10*

Table 1 – Computed parameters for all 4 states

Pressure volume loop analysis was performed for all 9 measurements. The obtained parameter values are given in table 1. Figure 17 shows a quick visual of the evolution of the computed parameters as the inotropic state changes.

Compared to baseline, E_{es} increased significantly with positive inotropic stimuli, but was not considerably changed with Esmolol. As discussed previously, the Esmolol measurement might not be a good representative of the corresponding state because it was recorded during a transitional state and does not represent steady state. The ESPVR of the Esmolol loop had even a higher slope than some of the baseline measurements. Figure 18 shows an example of PV loops representing the four states (Esmolol, baseline measurement n°4, Dobutamine 2.5, Dobutamine 5 measurement n°2) , as well their corresponding end-systolic elastances. The time to reach end systolic elastance T_{es} did however show a notable increase between baseline and Esmolol, but this is probably due to its heart rate dependency. $\frac{dP}{dt}_{max}$,on the other hand, was more sensitive to inotropic changes, it was reduced to half its value between baseline and Esmolol. During the period of Esmolol perfusion, the pressure

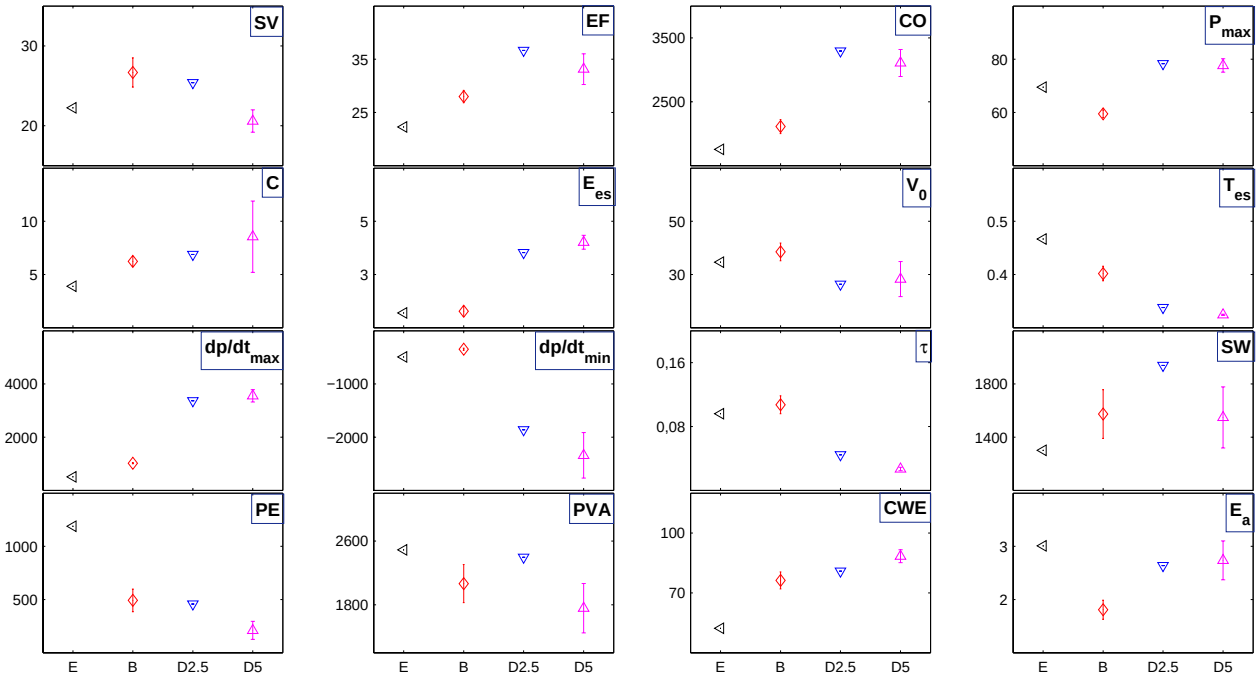

Figure 17 – Analysis parameters for all states

E: Esmolol , B : baseline, D2.5: Dobutamine 2.5 , D5 : Dobutamine 5

dynamics were able to slow down ($\frac{dP}{dt}_{max}$ decreased) but the pressure amplitude remained elevated, causing an elevated ESP, and thus an elevated E_{es}.

As expected, the diastolic compliance increased with inotropic enhancement. As contractility is increased, the PV loops shift to the left on the EDPVR, thus going towards smaller slopes (i.e. stiffness).

The stroke volume measurements confirmed that it is not a good contractility index. In fact, despite the contractility enhancement, because of its load dependency, the SV of the Dobutamine loop is smaller than that of baseline. Since the preload (EDV) decreased, so has the SV. The same can be argued for the EF which did not reflect the inotropic increase induced by the Dobutamine augmentation.

The relaxation process was sped up in response to Dobutamine. Both $\frac{dP}{dt}_{min}$ and τ decreased with positive inotropic stimuli. The expected opposite effect was, however, not observed for Esmolol. Relaxation for Esmolol remained faster than that of baseline. Note that the τ estimation for Dobutamine is error prone, the relaxation was very fast, leaving only a few points on the pressure relaxation curve for the exponential fitting.

Increasing the Dobutamine concentration did not enhance the stroke work (the SV decreased with an insignificant increase in maximum pressure), it did however somewhat enhance the cardiac work efficiency. Conversely, the CWE diminished notably with Esmolol.

The ESPVR axis intercept V_0 varies slightly among states but not distinctly enough to be attributed to contractility changes. Theoretically V_0 is independent of the inotropic state [24], all ESPVR and EDPVR should meet at the same axis intercept. The changes observed here account for the instability of V_0 [25] as well as measurement and estimation errors. Note that the V_0 range here is affected by the pressure offset and its correction.

The effective arterial elastance E_a increases with inotropic enhancement as ESP is increased. The ventriculoarterial coupling index E_a/E_{es} decreases when contractility increases. At baseline, this index is close to 1, indicating that the ventricle is working near maximal SW. With Dobutamine, E_a/E_{es}

is approximately 0.6, thus the heart is functioning around the optimal working point between maximal SW and maximal CWE, while remaining closer to maximal efficiency. During Esmolol perfusion, the coupling index is close to 2, the functioning mode is far from optimal, and widely inefficient.

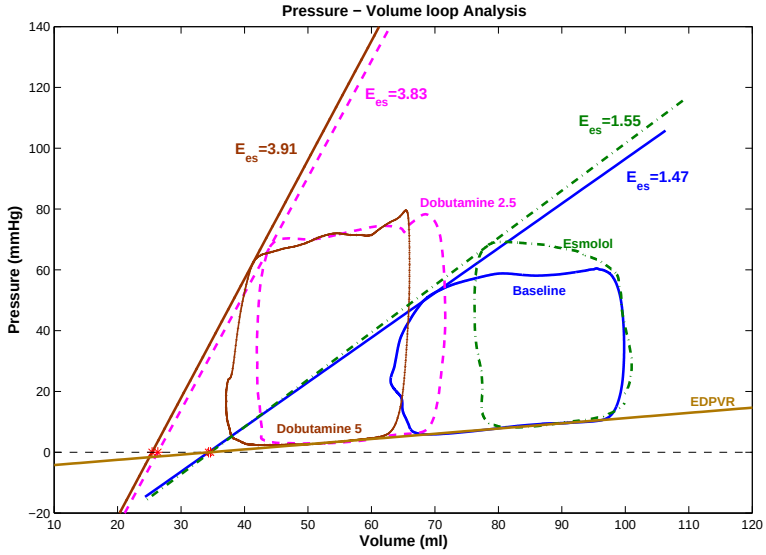

Figure 18 – End-systolic elastance for all contractility states

5.4 Principal component states representation

The PV loop analysis is done here by examining a large number of parameters N, some of which correlate with each other. Each loop is thus characterized by N variables. To represent a loop measurement, we need an N-dimensional space. However given that correlations exist between the parameters, the number of dimensions can be reduced using principle component analysis (PCA). With this method a new coordinate system is formed by new parameters which are derived as linear combinations of the old ones. A measurement can thus be represented by a reduced number of variables which are somewhat independent. Our computations have shown that the N parameters can be reduced to 3 or even 2 with no significant loss. Figure 19 shows the 9 measurements projected on a 3D and a 2D coordinate system, where the axis are linear combinations of the N parameters. This allows the visualization of sate clusters where the measurements corresponding to the same state are grouped.

This PCA procedure can be exploited for measurement classification. Having derived the principle component from a training set of measurements (such as we have here), given a new measurement we could, with a classification scheme, determine in which state the measurement has been recorded.

6 Discussion

MRI is considered to be the gold standard for absolute cardiac volume measurements. Obtaining PV loops requires simultaneously recording pressure during the MRI sessions. Pattynama *et al.*[47] used a Millar micromanometer to achieve such measurements, and argued that because it is made from

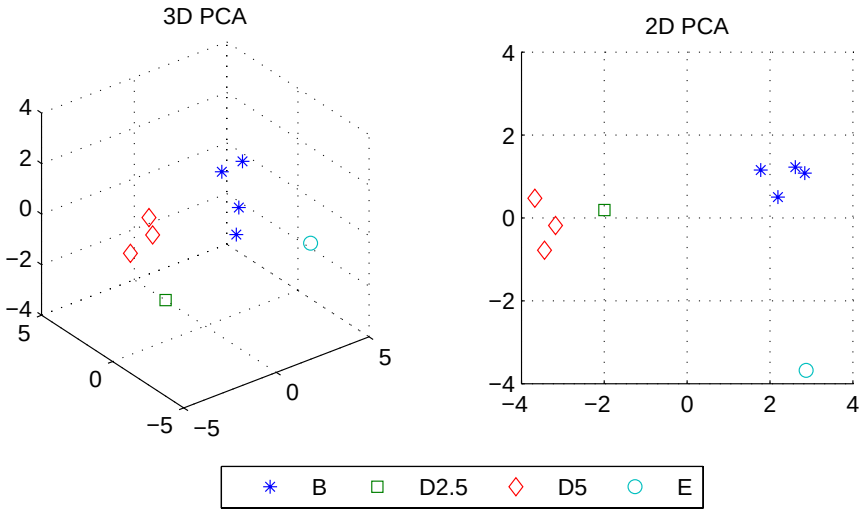

Figure 19 – 2D and 3D representation by principal component analysis

brass the obtained pressure signals were not significantly altered, however, some image artifacts were observed. Schmitt *et al.*[48] and Kuehne *et al.*[49] used liquid filled catheters to measure ventricular pressure down a 1m pressure line. The impedance of the transmission line reduces pressure amplitudes, and constitutes a low pass filter that attenuates high frequency components. A pressure sensor placed inside the ventricle would provide a more accurate representation of the actual LV pressure. The use of optical sensors in this study enabled pressure measurements directly in the ventricle without any interaction with the MRI acquisition.

Study limitations

- ▷ Unlike the conductance catheter technique, PV loop calculation using MRI imposes the use of an average pressure cycle vs average volume instead of instantaneous pressure vs instantaneous volume. Thus, the PV loop here reflects a global performance cycle and does not take into account an exact punctual correspondence between individual volume and a pressure measurements.Moreover the time synchronization between the volume and pressure cycle in this study was done based on bibliographic data, a more accurate match could be achieved by using the pressure signal to trigger the image acquisition and thus synchronize both waveforms.
- ▷ Due to the lack of real-time volume recordings, it was impossible to obtain a series of load varying PV loops using MRI because a steady state over several cycles is needed in order to compute a volume. For the same reason, the assessment of contractility transit states is not possible using MRI. This remains, for now, an advantage in favor of the conductance technique, however, future advances in MRI may enable the overcoming of this limitation.
- ▷ An attempt to correct the pressure offset was made here but pressure values might not be representatives of the real values. If we assume that we only have an additive offset term on pressure, some parameters can still be considered accurate despite the unknown offset, such as E_{es} , C ,SW , τ, ... Other parameters, however, such as V_0, PE, E_a necessitate the knowledge of the real offset value. There might also be an amplification term in the pressure sensors, this would have further effects on the estimated parameters. The pressure sensors need to be characterized and their behavior must be modeled to correct pressure measurements

- ▷ The computed PV loop indexes depend greatly on the measurement accuracy, whether MR volume estimations, or pressure sensor accuracy. We don't really have an assessment of either.
- ▷ A more comprehensive study including several animals must be carried out to confirm the results and conclusions given here.

List of abbreviations

CO	Cardiac Output
CWE	Cardiac Work Efficiency
EDP	End Diastolic Pressure
EDPVR	End-Diastolic Pressure-Volume Relationship
EDV	End Diastolic Volume
EF	Ejection Fraction
ESP	End Systolic Pressure
ESPVR	End-Systolic Pressure-Volume Relationship
ESV	End-Systolic Volume
HR	Heart Rate
IC	Isovolumic Contraction
IR	Isovolumic Relaxation
LV	Left Ventricle
LVP	Left Ventricle Pressure
MR	Magnetic Resonance
MRI	Magnetic Resonance Imaging
PE	Potential Energy
PRSW	Preload Recruitable Stroke Work
PV	Pressure-Volume
PVA	Pressure Volume Area
SV	Stroke Volume
SW	Stroke Work
VCO	Vena Cava Occlusion

References

[1] M. Maeder and D. Kaye. Heart failure with normal left ventricular ejection fraction. *J. Am. Coll. Cardiol.*, 53(11):905 – 918, 2009.

[2] K. Gaddam and S. Oparil. Diastolic dysfunction and heart failure with preserved ejection fraction: rationale for raas antagonist/ccb combination therapy. *Am J Hypertens*, 3(1):52 – 68, 2009.

[3] W. Grossman, F. Haynes, J. Paraskos, S. Saltz, J. Dalen, and L. Dexter. Alterations in preload and myocardial mechanics in the dog and in man. *Circ. Res.*, 31:83–94, 1972.

[4] D. Kass, W. Maughan, Z. Guo, A. Kono, K. Sunagawa, and K. Sagawa. Comparative influence of load versus inotropic states on indexes of ventricular contractility: experimental and theoretical analysis based on pressure-volume. *Circulation*, 76:1422–1436, 1987.

[5] D. Mason, E. Braunwald, J. Covell, E. Sonnenblick, and J. Ross. Assessment of cardiac contractility: The relation between the rate of pressure rise and ventricular pressure during isovolumic systole. *Circulation*, 44:47–58, 1971.

[6] P. Cohn, A. Liedtke, J. Serur, and E. Sonnenblick. Maximal rate of pressure fall (peak negative dp/dt) during ventricular relaxation. *Cardiovasc. Res.*, 6:263–267, 1972.

[7] J. Weiss, J. Frederisken, and M. Weisfeldt. Hemodynamic determinants of the time-course of fall in canine left ventricular pressure. *J. Clin. Invest.*, 58:751–760, 1976.

[8] S. Varma, R. Owen, M. Smucker, and M. Feldman. Is tau a preload-independent measure of isovolumetric relaxation? *Circulation*, 80:1757–1765, 1989.

[9] W. Little. The left ventricular dp/dt max -end-diastolic volume relation in closed-chest dogs. *Circ. Res.*, 56:808–815, 1985.

[10] M. Zile and D. Brutsaert. New concepts in diastolic dysfunction and diastolic heart failure: Part I:diagnosis, prognosis, and measurements of diastolic function. *Circulation*, 105:1387–1393, 2002.

[11] E. Brinke, R. Klauts, H. Verwey, E. van der Wall, R. Dion, and P. Steendijk. Single-beat estimation of the left ventricular end-systolic pressure-volume relationship in patients with heart failure. *Acta Physiol.*, 198:37–46, 2010.

[12] H Suga. Global cardiac function: mechano-energetico-informatics. *J. Biomech*, 36(5):713–720, May 2003.

[13] K. Hayashida, K. Sunagawa, M. Noma, M. Sugimachi, H. Ando, and M. Nakamura. Mechanical matching of the left ventricle with the arterial system in exercising dogs. *Circ. Res.*, 71:481–489, 1992.

[14] R. Kelly, C. Ting, T. Yang, C. Liu, W. Maughan, M. Chang, and D. Kass. Effective arterial elastance as index of arterial vascular load in humans. *Circulation*, 86:513–521, 1992.

[15] M. Danton, G. Greil, J. Byrne, M. Hsin, L. Cohn, and S. Maier. Right ventricular volume measurement by conductance catheter. *Am. J. Physiol.-Heart C.*, 285:1774–1785, 2003.

[16] C Jacoby, A Molojavyi, U Flogel, MW Merx, ZP Ding, and J Schrader. Direct comparison of magnetic resonance imaging and conductance microcatheter in the evaluation of left ventricular function in mice. *Basic Res. Cardiol.*, 101(1):87–95, JAN 2006.

[17] E. M. Winter, R. W. Grauss, D. E. Atsma, B. Hogers, R. E. Poelmann, R. J. van der Geest, C. Tschope, M. J. Schalij, A. C. Gittenberger-de Groot, and P. Steendijk. Left ventricular function in the post-infarct failing mouse heart by magnetic resonance imaging and conductance catheter: a comparative analysis. *Acta Physiol.*, 194(2):111–122, OCT 2008.

[18] S. Glantz and R. Kernoff. Muscle stiffness determined from canine left ventricular pressure-volume curves. *Circ. Res.*, 37:787–794, 1975.

[19] J. Gilbert and Glantz S. Determinants of left ventricular filling and of the diastolic pressure-volume relation. *Circ. Res.*, 64:827–852, 1989.

[20] M. Dickstein, O. Yano, H. Spotnitz, and D. Burkhoff. Assessment of right ventricular contractile state with the conductance catheter technique in the pig. *Cardiovasc. Res.*, 29:820–826, 1995.

[21] J. Thomas and A. Weyman. Echocardiographic doppler evaluation of left ventricular diastolic function. physics and physiology. *Circulation*, 84:977–990, 1991.

[22] W. Grossman, E. Braunwald, T. Mann, L. Mclaurin, and L. Green. Contractile state of the left ventricle in man as evaluated from end-systolic pressure-volume relations. *Circulation*, 56:845–852, 1977.

[23] H. Mehmel, B. Stockins, K. Ruffmann, K. von Olshausen, G. Schuler, and W. Kubler. The linearity of the end-systolic pressure-volume relationship in man and its sensitivity for assessment of left ventricular function. *Circulation*, 63:1216–1222, 1981.

[24] H. Suga, K. Sagawa, and A. Shoukas. Load independence of the instantaneous pressure-volume ratio of the canine left ventricle and effects of epinephrine and heart rate on the ratio. *Circ. Res.*, 32:314–322, 1973.

[25] J. Spratt, G. Tyson, D. Glower, J. Davis, L. Muhlbaier, C. Olsen, and J. Rankin. The end-systolic pressure-volume relationship in conscious dogs. *Circulation*, 75:1295–1309, 1987.

[26] M. Takeuchi, Y. Igarashi, S. Tomimoto, M. Odake, T. Hayashi, T. Tsukamoto, K. Hata, H. Takaoka, and H. Fukuzaki. Single-beat estimation of the slope of the end-systolic pressure-volume relation in the human left ventricle. *Circulation*, 83:202–212, 1991.

[27] H. Senzaki, C. Chen, and D. Kass. Single-beat estimation of end-systolic pressure-volume relation in humans. *Circulation*, 94:2497–2506, 1996.

[28] T. Shishido, K. Hayashi, K. Shigemi, T. Sato, M. Sugimachi, and K. Sunagawa. Single-beat estimation of end-systolic elastance using bilinearly approximated time-varying elastance curve. *Circulation*, 102:1983–2989, 2000.

[29] C. Chen, B. Fetics, E. Nevo, C. Rochitte, K. Chiou, P. Ding, M. Kawagachi, and D. Kass. Nonunvaasive single-beat determination of left ventricular end-systolic elastance in humans. *J. Am. Coll. Cardiol.*, 38:2028–2034, 2001.

[30] K. Kjorstad, C. Korvald, and T. Myrmel. Pressure-volume-based single-beat estimations cannot predict left ventricular contractility in vivo. *Am. J. Physiol.-Heart C.*, 282:1739–1750, 2001.

[31] W. Little, C.P. Cheng, M. Mumma, Y. Igarashi, J. Vinten-Johansen, and W. Johnston. Comparison of measures of left ventricular contractile performance derived from presure-volume loops in conscious dogs. *Circulation*, 80:1378–1387, 1989.

[32] K. Sunagawa, W. Maughan, and K. Sagawa. Optimal arterial resistance for the maximal stroke work studied in isolated canine left ventricle. *Circ. Res.*, 56:586–595, 1985.

[33] D. Glower, J. Spratt, N. Snow, J. Kabas, J. Davis, C. Olsen, G. Tyson, Sabiston D., and J. Rankin. Linearity of the frank-starling relationship in the intact heart : the concept of preload recruitable stroke work. *Circulation*, 71:994–1009, 1985.

[34] K. Mohanraj and M. Feneley. Single-beat determination of preload recruitable stroke work relationship:derivation and evaluation in conscious dogs. *J Am Coll Cardiol.*, 35:502–513, 2000.

[35] T. Kameyama, H. Asanoi, S. Ishizaka, K. Yamanishi, M. Fujita, and S. Sasayama. Energy conversion efficiency in human left ventricle. *Circulation*, 85:988–996, 1992.

[36] T. Nozawa, Y. Yasumura, S. Futaki, N. Tanaka, M. Uenishi, and H Suga. Efficiency of energy transfer from pressure-volume area to external mechanical work increases with contractile state and decreases with afterload in the left ventricle of the anesthetized closed-chest dog. *Circulation*, 77:1116–1124, 1988.

[37] M. Starling. Left ventricular-arterial coupling relations in the normal human heart. *Am. Heart J.*, 125:1659–1666, 1993.

[38] H. Asanoi, S. Sasayama, and T. Kameyama. Ventriculoarterial coupling in normal and failing heart in humans. *Circ. Res.*, 65:483–493, 1989.

[39] NB Charan, R Ripley, and P Carvalho. Effect of increased coronary venous pressure on left ventricular function in sheep. *Resp. Physiol.*, 112(2):227–235, MAY 1998.

[40] Lawrence S. Lee, Ravi K. Ghanta, Suyog A. Mokashi, Otavio Coelho-Filho, Raymond Y. Kwong, R. Morton Bolman, III, and Frederick Y. Chen. Ventricular restraint therapy for heart failure: The right ventricle is different from the left ventricle. *J. Thorac. Cardiovasc. Surg.*, 139(4):1012–1018, APR 2010. 35th Annual Meeting of the Western-Thoracic-Surgical-Association, Banff, CANADA, JUN 24-27, 2009.

[41] F Bauer, M Jones, T Shiota, MS Firstenberg, JX Qin, H Tsujino, YJ Kim, M Sitges, LA Cardon, AD Zetts, and JD Thomas. Left ventricular outflow tract mean systolic acceleration as a surrogate for the slope of the left ventricular end-systolic pressure-volume relationship. *J. Am. Coll. Cardiol.*, 40(7):1320–1327, OCT 2 2002.

[42] MB Ratcliffe, AW Wallace, A Salahieh, J Hong, S Ruch, and TS Hall. Ventricular volume, chamber stiffness, and function after anteroapical aneurysm plication in the sheep. *J. Thorac. Cardiovasc. Surg.*, 119(1):115–124, JAN 2000.

[43] JJ Pilla, AS Blom, DJ Brockman, VA Ferrari, D Yuan, and MA Acker. Passive ventricular constraint to improve left ventricular function and mechanics in an ovine model of heart failure secondary to acute myocardial infarction. *J. Thorac. Cardiovasc. Surg.*, 126(5):1467–1476, NOV 2003.

[44] P Segers, P Steendijk, N Stergiopulos, and N Westerhof. Predicting systolic and diastolic aortic blood pressure and stroke volume in the intact sheep. *J. Biomech.*, 34(1):41–50, JAN 2001.

[45] G. Diamond, J. Forrester, J. Hargis, W. Parmley, R. Danzig, and Swan J. Diastolic pressure-volume relationship in the canine left ventricle. *Circ. Res.*, 29:267–275, 1971.

[46] J. Forrester, G. Diamond, W. Parmley, and Swan J. Early increase in left ventricular complinace after myocardial infarction. *J. Clin. Invest.*, 51:598–603, 1972.

[47] P. Pattynama, A Deroos, E Vandervelde, H Lamb, P Steendijk, J Hermans, and J Baan. Magnetic-Resonance-Imaging Analysis Of Left-ventricular Pressure-Volume Relations - Validation With The Conductance Method At Rest And During Dobutamine Stress. *Magn. Reson. Med.*, 34(5):728–737, NOV 1995.

[48] B. Schmitt, P. Steendijk, K. Lunze, S. Ovroutski, J. Falkenberg, P. Rahmanzadeh, N. Maarouf, P. Ewert, F. Berger, and T. Kuehne. Integrated assessment of diastolic and systolic ventricular function using diagnostic cardiac magnetic resonance catheterization: Validation in pigs and application in a clinical pilot study. *J. Am. Coll. Cardiol. Img.*, 2:1271–1281, 2009.

[49] T. Kuehne, S. Yilmaz, P. Steendijk, P Moore, M. Groenink, M. Saaed, O. Weber, C. Higgins, P. Ewret, E. Fleck, I. Nagel, E. Schulze-Neick, and P. Lange. Magnetic resonance imaging analysis of right ventricular pressure-volume loops: In vivo validation and clinical application in patients with pulmonary hypertension. *Circulation*, 110:2010–2016, 2004.